Experimental Demonstration and Characterization of a Non-Mode Selective (De)Multiplexer Using Multi-Plane Light Converter (MPLC)

Shree R. Thapa, Seth Smith-Dryden, Zheyuan Zhu, Shuo S. Pang, and Guifang Li

***Abstract*—We experimentally demonstrate the use of a multi-plane light converter (MPLC) as a non-mode selective (de)multiplexer for converting Hermite-Gaussian (HG) modes into a Hadamard matrix of fundamental Gaussian spots and vice versa. We interferometrically measure and characterize the complex output of the device and successfully demonstrate the conversion between HG modes and Hadamard matrices of Gaussian spots. The MPLC non-mode selective (de)multiplexers can be useful for versatile control of spatial properties of light beams with potential applications in beam shaping, coherent beam combining, and wavefront synthesis.**

***Index Terms*—MPLC, Hadamard matrix, Hermite-Gaussian mode, mode (de)multiplexer.**

I. Introduction

MPLCS are optical devices that theoretically perform lossless unitary conversions [1], [2]. The ability to perform efficient, accurate conversions makes MPLCs highly desirable for mode-selective (MS) (de)multiplexing applications, where each input is mapped to one and only one of orthogonal output modes. MS MPLCs have been used extensively in space-division multiplexed optical communications systems [3], [4], [5]. In addition, non-mode-selective (NMS) MPLCs have been proposed, where a particular combination of multiple inputs, which can be considered as a supermode, is mapped to a particular orthogonal output mode [6]. In this case, one input combination is orthogonal to another.

Using an NMS MPLC has shown an advantage over its MS counterpart particularly for beam combining with imperfect phase-locking [7]. In that study, a linear Hadamard array was mapped to structurally similar HG modes. Recently, we designed an NMS MPLC MUX for a two-dimensional (2D) input array [6], [8]. These devices are expected to be useful for beam combining of 2D emitters with imperfect phase-locking. Furthermore, using a set of 2D supermodes comprised of square Hadamard-coded spot arrays, the NMS MPLCs can produce a corresponding set of Hermite-Gaussian (HG) modes. Consequently, in addition to beam combining, NMS MPLCs can be used for beam shaping, beam steering and wavefront control.

In this paper, we present the design and experimental validation of an MPLC system operated as an NMS demultiplexer (De-MUX). The primary purpose of this NMS MPLC De-MUX is to split a set of HG modes into a Hadamard array of fundamental Gaussian spots. By taking advantage of the reciprocal nature of MPLC systems [9], [10], [11], the same device can also function as an NMS MUX for coherent beam combining.

II. Design and Numerical Validation of MPLC-Based NMS De-MUX

The MPLC in this study is composed of sets of phase masks and a planar reflective mirror, which together form a multi-pass cavity in free space, as shown in Fig. 1. The phase masks within the MPLC cavity provide successive phase modulations, leading to an adiabatic conversion of the wavefront [12].

The wavefront matching method has been employed to generate the phase masks used in MPLC designs and experiments [13]. The wavefront matching method involves a process of iteratively adjusting the phase distribution of a phase mask to match the desired wavefront. This is typically done by comparing the measured wavefront with the target wavefront and iteratively optimizing the phase mask until a good match is achieved [14]. The wavefront-matching algorithm uses the conjugate input light field $u_{in}*$ to calculate the corrective phase distribution. This corrective phase distribution is then applied to the incoming light field, resulting in the output light field u_{out}. To obtain the phase distribution Φ for a given phase masks, the algorithm iteratively computes a corrective phase distribution given by

$$\Delta\Phi = \arg\left(\sum_{i=1}^{N} {u_{in,i}}^{*} u_{out,i}\right) \tag{1}$$

until the measured wavefront matches a desired reference wavefront. In (1), N represents the number of supported modes. The angular spectrum algorithm is typically utilized to calculate both the input light field and the output light field.

The phase masks in MPLC can be realized using spatial light modulators or phase plates fabricated using grayscale lithography. In grayscale lithography phase delay at each pixel, Φ, is related to the etching depth (h) by $h = \Phi * \lambda / (4\pi)$, where λ represents the wavelength of the light being used [15]. Grayscale

Manuscript received 11 January 2024; revised 26 February 2024; accepted 10 March 2024. Date of publication 19 March 2024; date of current version 1 April 2024. This work was supported in part by Army Research Lab under Grant W911NF1920265, and in part by the Office of Naval Research under Grant N00014-22-1-2237. *(Corresponding author: Shree R. Thapa.)*

The authors are with the CREOL, The College of Optics and Photonics, University of Central Florida, Orlando, FL 32816 USA (e-mail: shree.ram.thapa@ucf.edu; seth.smith-dryden@ucf.edu; zheyuan.zhu@ucf.edu; pang@ucf.edu; li@ucf.edu).

Digital Object Identifier 10.1109/JPHOT.2024.3377705

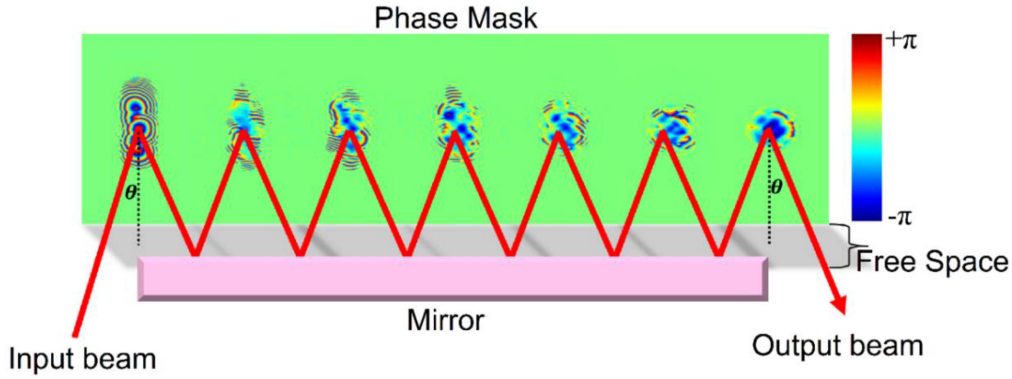

Fig. 1. Schematic diagram of a reflective MPLC with an incident angle (θ) for the input beam.

lithography can achieve higher resolution (smaller pixel size) and much large phase masks (larger area/number of pixels), and therefore much better performances [16]. However, once the phase plates are fabricated by grayscale lithography, they are fixed and cannot be modified. On the other hand, SLMs offer the advantage of adaptive tuning of mask designs, and they are very useful for design verification. In this paper, we design, through simulations, phase masks corresponding to the parameters of grayscale lithography and SLM. These simulation results indicate the potential performance metrics of the NMS MPLCs. In addition, the designed masks corresponding to the parameters of SLMs were experimentally tested to verify the designs.

The parameters used for comparing the design performance of both (SLM and grayscale lithography) phase modulation approaches are as follows. In the simulations, the pixel sizes for the phase plate and SLM were set at 6 μm, and 8 μm, respectively, to be consistent with experimental conditions. To make the overall size of the phase screens for the phase plate and SLM nearly identical for fair comparisons, the number of pixels used were 350 by 350 and 265 by 265, respectively for the phase plate, and the SLM. All simulations used 7 phase masks. The output beams are encoded using Hadamard coding and arranged in a 4 $\times$ 4 square configuration, as shown in Fig. 2. All input beams have the same power and a mode field diameter (MFD) of 116.36 μm.

The output beams with MFD of 30 μm are spaced apart by 36 um. The phase of each input beam is either 0 or π, resulting in field amplitudes of $+1$ or -1. Each input beam represents a specific element of the Hadamard codewords, forming a 16-bit code. The Hadamard code set consists of 16 codewords, where each code is mutually orthogonal. The performance of the NMS De-MUX is evaluated through a coupling matrix C that assesses the similarity between the simulated output field profiles and the desired ones. Each element of the coupling matrix C for comparing the simulated complex output field profiles ($u_{actual,i}(x,y)$) to the complex conjugate of desired/ideal field ($u_{desired,j}(x,y)$) is the overlapping integral given by

$$C_{ij} = \frac{\iint u_{actual,i}(x,y) \times u^{*}_{desired,j}(x,y)\, dxdy}{\iint |u_{actual,i}(x,y)|^{2} dxdy} \quad (2)$$

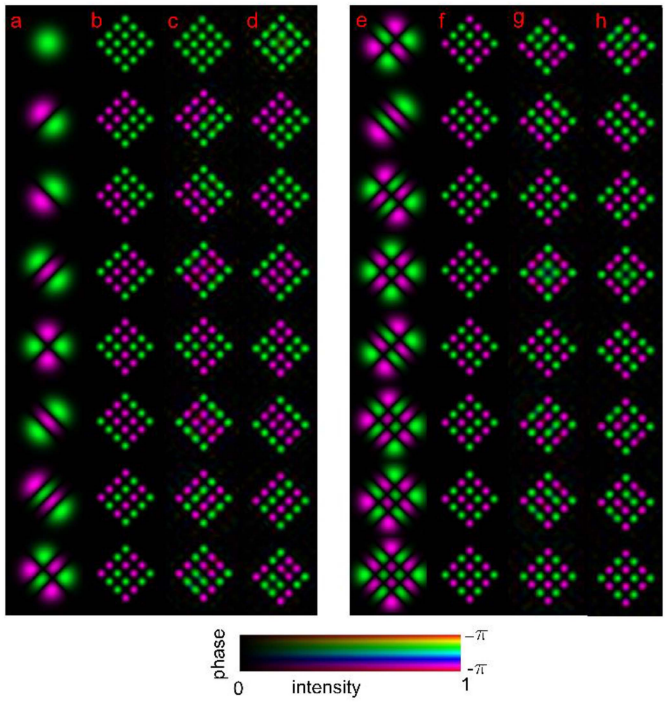

Fig. 2. Comparison of the ideal outputs and simulated output using NMS MPLC De-MUX: (a) and (e) illustrate the input HG fields with MFD 450 μm. (b) and (f) are the desired output fields, (c) and (g) are the simulated outputs using the SLM-based NMS MPLC De-MUX, (d) and (h) are the simulated outputs using phase plate-based NMS MPLC De-MUX.

where x and y represent the dimension of the fields. The magnitude of the coupling matrices for the NMS MPLCs based on phase plates and SLMs are shown in Fig. 3(a) and (b), respectively. Insertion Loss (IL) and Mode-dependent Loss (MDL) are calculated as

$$\mathrm{IL} = \frac{1}{N}\sum_{n=1}^{N} |S_n|^2 \quad (3)$$

$$\mathrm{MDL} = \frac{\max(|S_n|^2)}{\min(|S_n|^2)} \quad (4)$$

where Sn are the singular values of the complex coupling matrix. They are shown in Fig. 3(c) and (d), for the NMS MPLCs based

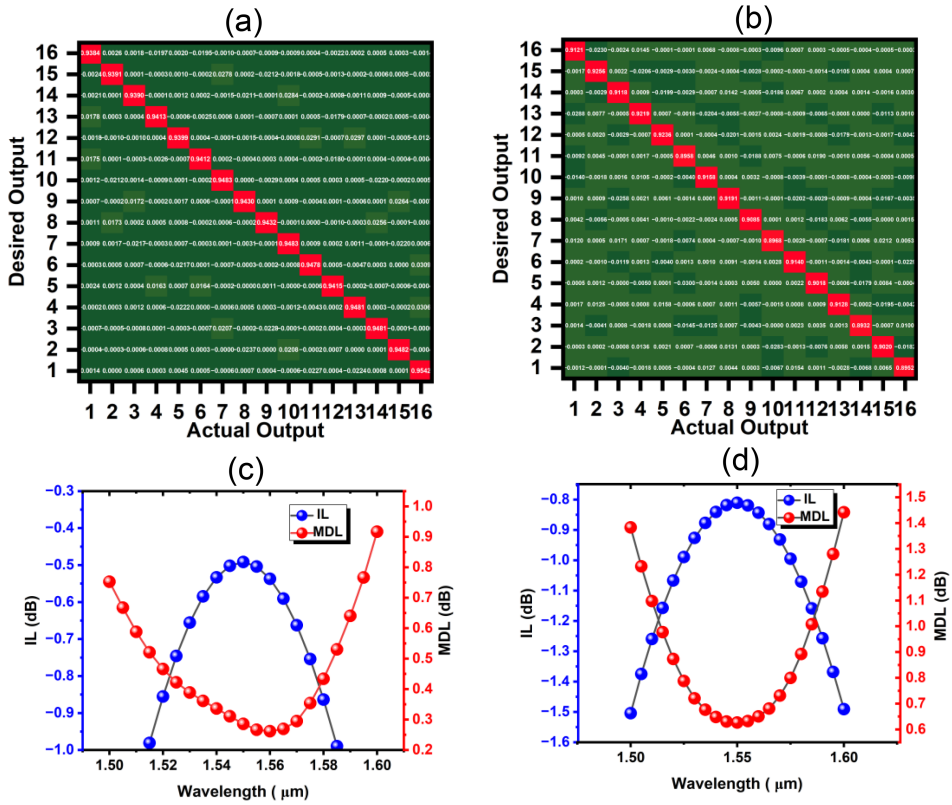

Fig. 3. Simulated coupling matrix, IL and MDL: (a) and (c) phase plate-based NMS MPLC De-MUX, (b) and (d) SLM-based NMS MPLC De-MUX. The red parts in the coupling matrix C highlight its diagonals.

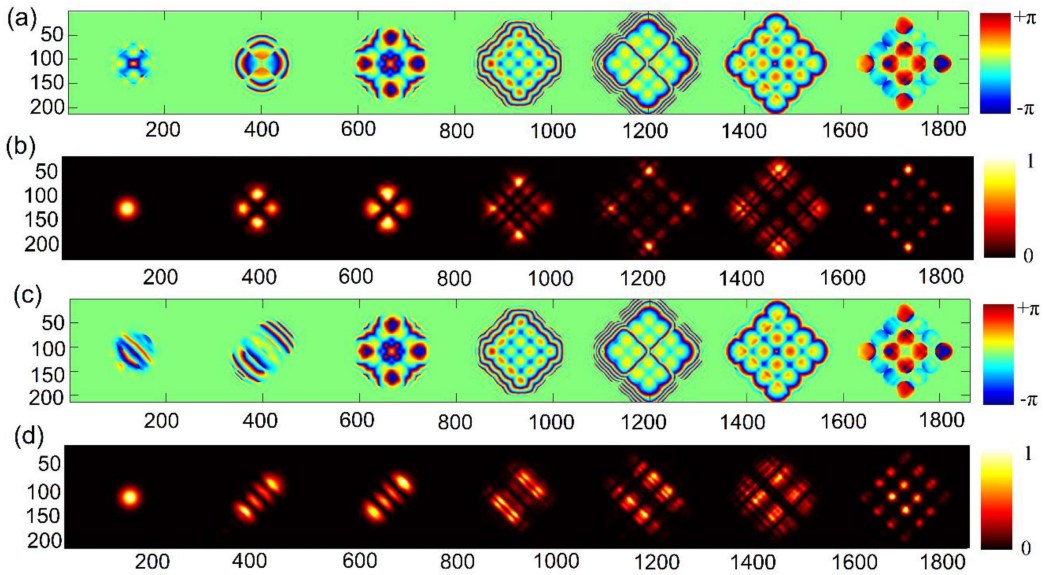

Fig. 4. Phase masks and simulated light fields tailored for specific HG modes. In panels (a) and (c), the phase masks reveal the combined system from stages 1 and 2, designed for HG_{11} and HG_{30} modes, respectively. Conversely, panels (b) and (d) showcase the simulated light fields propagating in the direction of propagation, resulting from the interaction of the input field with the respective masks designed HG_{11} and HG_{30} modes.

on phase plates and SLMs, respectively. The IL and MDL for the phase plate approach are -0.483 dB and 0.251 dB, respectively, at 1550 nm. On the other hand, for the SLM approach, the IL and MDL are -0.795 dB and 0.591 dB, respectively.

Using smaller pixel sizes for the phase modulations provides a higher spatial resolution, allowing for finer control and manipulation of the optical field. This enhanced control leads to improved performance in terms of IL and MDL. Furthermore,

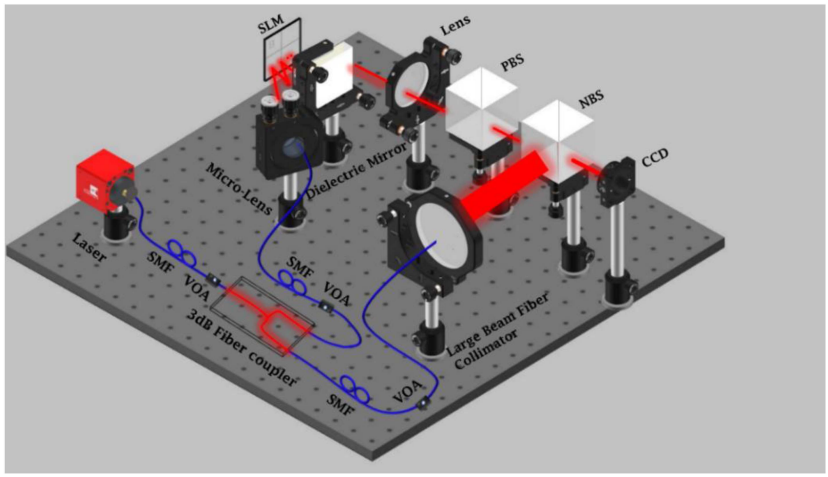

Fig. 5. Schematic diagram of the experimental setup for the NMS MPLC De-MUX and off-axis digital holography to reconstruct the amplitude and phase of the output field from NMS De-MUX using SLM.

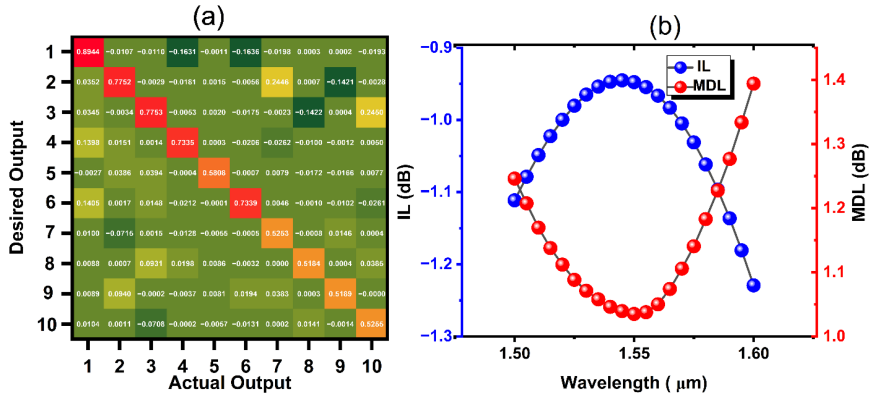

Fig. 6. Performances (simulation) for the combined system stage 1 and stage 2: (a) coupling matrix and (b) IL and MDL.

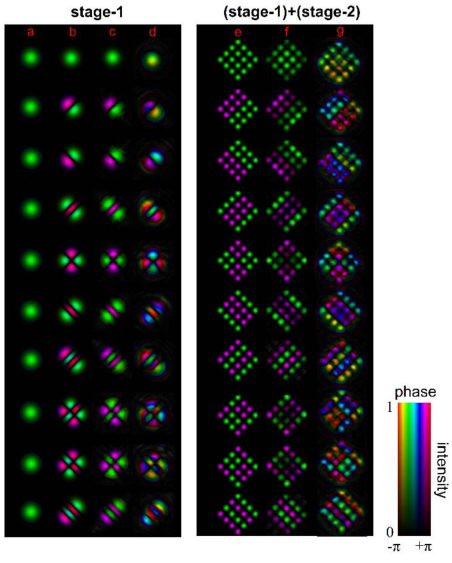

Fig. 7. Comparison of the simulation and experimental results for stage 1 and combined system of stage 1 and stage 2: (a), (b), (c), and (d) are the input field, desired output, numerically calculated output, and experimental output fields, respectively, for stage 1; (e), (f), and (g) are the desired output, numerically calculated output, and the experimentally reconstructed output field obtained from the combined system of stage 1 and stage 2.

increasing the number of phase masks, which is possible using phase plates, usually yields better performance.

III. Experimental Validation of MPLC-Based NMS De-MUX Using SLM

To validate NMS MUX/De-MUX designs, we used an SLM for experimental demonstrations. The SLM allows us to customize and implement different sets of phase masks, providing flexibility in evaluating and verifying the performance of the NMS De-MUX. For our experimental validation, we elected to use a Holoeye PLUTO 2.1 SLM which contains 1920×1080 pixels.

The pixel size of the SLM is 8 μm. The SLM can simultaneously display up to 7 265×512 phase masks. The first two phase masks were used to convert the input fundamental Gaussian mode into a desired HG mode. We refer to this converter as "Stage 1". The other 5 phase masks were used for the NMS De-MUX, which we refer to as "Stage 2". Due to the limited total number of pixels of the SLM, Stage 2 could only support up to the first 10 HG modes. To couple different HG modes into Stage 2, the phase masks in Stage 1 were updated accordingly. The combined 7-mask system consisting of both stages is shown

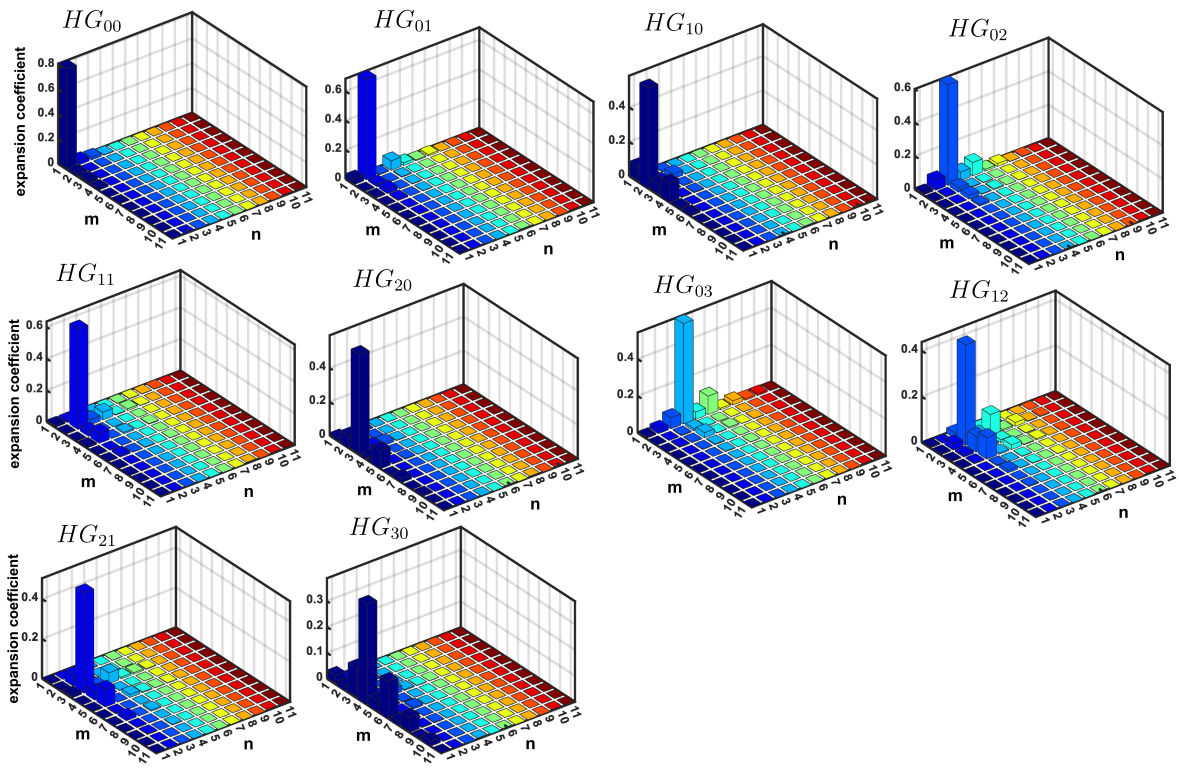

Fig. 8. Illustration depicts the computation of mode expansion coefficients for a measured experimental array consisting of 16 spots, all generated using the derived holographic patterns and employing the same phase mask as in stage 2. For instance, in the top-left figure, approximately 80% of the 16 measured spots exhibit both uniform phase and equal amplitude with respect to all the derived output patterns from stage 2. The modes are labeled from #1, representing the fundamental mode, HG_{00}, and subsequent modes follow in order.

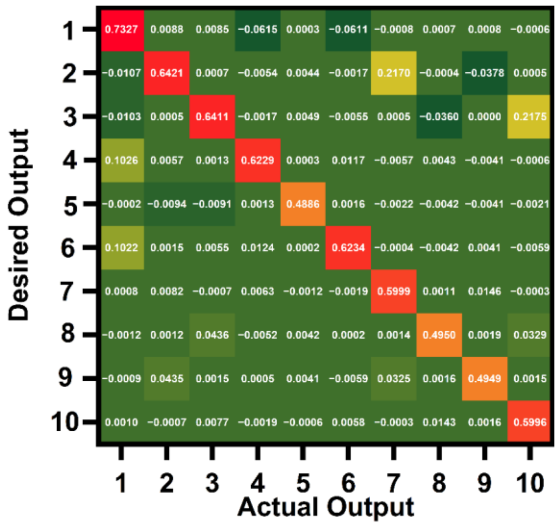

Fig. 9. Amplitude of coupling matrix with desired 16 hadamard pattern spots calculated with experimental measured outputs.

in Fig. 4. The experimental setup, shown in Fig. 5, uses a Mach-Zehnder interferometer to holographically record the amplitude and phase information of the MPLC outputs [2]. The input into Stage 1 is a collimated Gaussian beam of MFD 320 μm at $\lambda = 1550$ nm.

The performances of the experiment are presented in Fig. 6. The IL and MDL at $\lambda = 1550$ nm are -0.947 dB and 1.035 dB, respectively for the combined system. Fig. 7 shows the comparison between the simulation results and experimental results for both Stage 1 and the combined system of Stage 1 and Stage 2.

To quantitatively analyze the performance, Fig. 8 illustrates the calculated mode expansion coefficients, which serve to assess the purity of the HG modes produced experimentally for Stage 1. These coefficients provide insights into the degree of similarity between the ideal HG modes and the corresponding measured outputs for each specific mode. Notably, in Fig. 8, the HG_{00} mode demonstrates an 80% similarity between the measured output and the desired ideal output. This similarity is determined using (2), where '$u_{desired}$' encapsulates all potential ideal outputs from Fig. 7(e), and 'u_{actual}' refers to the experimentally retrieved complex field (specifically, the first column element of Fig. 7(g)) obtained from off-axis digital holography. However, for the HG_{11} mode, a similarity of only 58% was achieved, indicating that the remaining field components are a mixture of other possible outputs from Fig. 7(e). These findings suggest that the output obtained from Stage 1 deviates from the ideal desired mode for Stage 2. In Stage 2, phase masks are designed assuming that the input HG field is ideal. Consequently, the experimental performance achieved by the combined system of Stage 1 and Stage 2 may be poorer than the simulated outputs for the respective HG modes, especially for those mode that have lower similarities for Stage 1. The complex coupling matrix between the ideal output and the experimentally obtained output, as illustrated in Fig. 7(e) and (g), was calculated then plotted in Fig. 9. Singular value decomposition (SVD) was applied, and (3) and (4) were again utilized to compute the IL and

MDL. From these calculations, IL and MDL were determined to be −2.53 dB and 1.630 dB, respectively. These values serve as quantitative indicators, providing insights into the extent of signal loss and mode-dependent loss in the output compared to the ideal outputs.

IV. Conclusion

This study experimentally validated the recently proposed non-mode selective (de)multiplexing technique using MPLC. Through a combination of simulations and experiments, we have successfully demonstrated the conversion of HG modes into corresponding Hadamard array patterns. The performance of MPLCs was evaluated by comparing the interferometrically-measured output patterns with their ideal counterparts. By incorporating more phase masks into the MPLC, we anticipate further improvements in the performance of the NMS Mux/De-MUX.

Disclosures

The authors declare no conflicts of interest.

References

[1] G. Labroille et al., "Efficient and mode selective spatial mode multiplexer based on multi-plane light conversion," *Opt. Exp.*, vol. 22, pp. 15599–15607, 2014.

[2] N. K. Fontaine et al., "Laguerre-Gaussian mode sorter," *Nature Commun.*, vol. 10, 2019, Art. no. 1865.

[3] P. Genevaux et al., "6-mode spatial multiplexer with low loss and high selectivity for transmission over few mode fiber," in *Proc. Opt. Fiber Commun. Conf. Exhib.*, 2015, pp. 1–3.

[4] H. Wen, H. Liu, Y. Zhang, R. Sampson, S. Fan, and G. Li, "Scalable Hermite–Gaussian mode-demultiplexing hybrids," *Opt. Lett.*, vol. 45, pp. 2219–2222, 2020.

[5] N. Barré, B. Denolle, P. Jian, J. Morizur, and G. Labroille, "Broadband, mode-selective 15-mode multiplexer based on multi-plane light conversion," in *Proc. Opt. Fiber Commun. Conf. Exhib.*, 2017, pp. 1–3.

[6] H. Wen et al., "Scalable non-mode selective Hermite–Gaussian mode multiplexer based on multi-plane light conversion," *Photon. Res.*, vol. 9, pp. 88–97, 2021.

[7] A. Billaud et al., "Optimal coherent beam combining based on multi-plane light conversion for high throughput optical feeder links," in *Proc. IEEE Int. Conf. Space Opt. Syst. Appl.*, 2019, pp. 1–5.

[8] S. R. Thapa, S. Smith-Dryden, Z. Zhu, S. Pang, and G. Li, "Experimental demonstration of a non-mode selective MPLC (de)multiplexer," in *Proc. IEEE Photon. Conf.*, 2023, pp. 1–2, doi: 10.1109/IPC57732.2023.10360561.

[9] J. Fang et al., "Optical orbital angular momentum multiplexing communication via inversely designed multphase light conversion," *Photon. Res.*, vol. 10, pp. 2015–2023, 2022.

[10] G. Labroille et al., "Characterization and applications of spatial mode multiplexers based on multi-plane light conversion," *Opt. Fiber Technol.*, vol. 35, pp. 93–99, 2017.

[11] S. Bade et al., "Fabrication and characterization of a mode-selective 45-mode spatial multiplexer based on multi-plane light conversion," in *Proc. Opt. Fiber Commun. Conf. Expo.*, 2018, pp. 1–3.

[12] N. K. Fontaine et al., "Hermite-Gaussian mode multiplexer supporting 1035 modes," in *Proc. Opt. Fiber Commun. Conf. Exhib.*, 2021, pp. 1–3.

[13] J. Carpenter and N. K. Fontaine, "Multi-plane light conversion with low plane count," in *Proc. Conf. Lasers Electro-Opt. Europe Eur. Quantum Electron. Conf.*, 2017, Art. no. 1.

[14] Y. Sakamaki, T. Saida, T. Hashimoto, and H. Takahashi, "New optical waveguide design based on wavefront matching method," *J. Lightw. Technol.*, vol. 25, no. 11, pp. 3511–3518, Nov. 2007.

[15] Z. Li, S. Yu, and G. Zheng, "Advances in exploiting the degrees of freedom in nanostructured metasurface design: From 1 to 3 to more," *Nanophotonics*, vol. 9, no. 12, pp. 3699–3731, 2020.

[16] Y. Pang et al., "3D stretchable arch ribbon array fabricated via grayscale lithography," *Sci. Rep.*, vol. 6, 2016, Art. no. 28552.